RSC Applied Interfaces

ROYAL SOCIETY OF CHEMISTRY

PAPER

View Article Online
View Journal | View Issue

Check for updates

Cite this: *RSC Appl. Interfaces*, 2024, 1, 580

Green synthesis of a disordered N-doped carbonaceous aerogel from waste for the removal of over-the-counter drugs and environmental assessment†

Himanshu Asati, [a] Raka Mondal[b] and Kumud Malika Tripathi *[a]

As the world grapples with the growing threat of water pollution, a particular concern is the presence of pharmaceutical pollutants in our water sources. Advanced adsorption methods for the removal of over-the-counter pharmaceuticals from wastewater have yet to appear due to the complexity of adsorbent synthesis and the risk of introducing nanomaterial contaminants into water. Herein, the risk of secondary contamination was reduced by using a sustainable, cost-effective, self-standing and super hydrophobic 3D N-doped carbonaceous aerogel (N-CA). The N-CA was synthesized in a one-pot approach using waste jaggery as a raw material. N-CA has advantageous characteristics, such as ultralight and easily separable, environmental friendliness, high stability, economic feasibility and ease in synthesis. N-CA demonstrates remarkable adsorption efficiency towards the removal of emerging pollutants with varying structures under natural conditions. In just 40 minutes, N-CA removes ~96% of acetylsalicylic acid (ASP) and ~99% of acetaminophen (PCM) at room temperature. The maximum adsorption capacity (q_m) of N-CA was determined to be 138.6963 ± 7.8687 mg g^{-1} for ASP and 117.7856 ± 2.7219 mg g^{-1} for PCM. The recycling study of N-CA demonstrated that the PCM and ASP absorption was almost the same up to seven and five cycles, respectively. Additionally, enhanced germination of beans and healthy growth of plants were observed in treated water compared to ASP and PCM contaminated water. The observations from this study reveal the potential of waste biomass-based materials in water remediation and the value of treated water in many applications.

Received 13th February 2024,
Accepted 18th February 2024

DOI: 10.1039/d4lf00046c

rsc.li/RSCApplInter

1. Introduction

In recent decades, the quality of our precious water resources has faced a serious threat from a multitude of factors including commercial and non-commercial use of pharmaceuticals,[1] micro pollutants,[2] pesticides,[3] personal care products,[4] and industrial waste.[5,6] Water pollution has become a pressing concern with wide-ranging complications for the local environment and the public.[4] Pharmaceutical waste in water also threatens the quality of drinking water and most of the medicines are not persistent but daily-use medications may be pseudo-persistent due to continuous introduction to the environment.[6] Endocrine disrupting chemicals impose significant impact in the environment but they have been less explored as compared to other harmful toxicant classes like carcinogens.[7] The residues of pharmaceuticals are also categorized as "compounds of emerging concern" owing to their potential to cause considerable effect on ecosystems and human health.[6] The presence of pharmaceuticals such as acetylsalicylic acid or aspirin (ASP) and acetaminophen or paracetamol (PCM) in household and hospital wastewater can be responsible for the emergence of drug-resistant bacteria.[8,9] Additionally, the improper disposal or flushing of unused or expired medications can accumulate in groundwater sources.[10] Most wastewater treatment plants are unable to remove pharmaceuticals efficiently *via* several treatment methods.[11] One reason for the low pharmaceutical removal efficiency is the trapping effect of the urine matrix in wastewater.[1] Consequently, the implementation of adequate wastewater treatment strategies, the adoption of responsible disposal practices or remediation techniques and exploring more efficacious water purification approaches are essential to improve the environmental difficulties.

In pursuit of the same objective, adsorption,[12] photocatalysis,[13] activated sludge processes,[14] advanced

[a] *Department of Chemistry, Indian Institute of Petroleum & Energy, Visakhapatnam, Andhra Pradesh, 530003, India. E-mail: kumud20010@gmail.com, kumud@iipe.ac.in*
[b] *Department of Chemical Engineering, Indian Institute of Petroleum & Energy, Visakhapatnam, Andhra Pradesh, 530003, India*

† Electronic supplementary information (ESI) available. See DOI: https://doi.org/10.1039/d4lf00046c

oxidation processes (AOPs),[15] chemical coagulation and flocculation,[16] ozonation,[17] membrane bioreactors (MBRs),[18] reverse osmosis (RO), electrocoagulation[19] and advanced membrane filtration[20] emerge as promising technologies for the mitigation of emerging pollutant concentration in water and wastewater. Each method has its pros and cons; biological treatment involves expensive enzymes, bacteria, and fungi that are difficult to handle at the same time and needs proper storage and preservation systems.[21] Other methods are expensive and need further chemicals to treat pharmaceuticals present in water.[22]

Adsorption is considered as a highly efficient and widely applied method in wastewater treatment.[23–25] Its superiority lies in its remarkable removal efficiency, potential for regeneration and reusability, ease of implementation, cost-effectiveness, vast collection of available adsorbent materials, absence of chemical additives, adaptability to diverse conditions, and its ability to complement other treatment methods.[26–28] Various adsorbent materials find application in wastewater treatment to proficiently eliminate contaminants. Among the frequently utilized ones are activated carbon,[29] zeolites,[30] clay minerals,[31] activated alumina,[32] biosorbents,[33] carbon nanotubes,[34] polymeric resins,[35] hydrous iron oxides,[36] silica gel,[37] and nano-carbons.[38] The chemical stability, high specific surface area, recyclability and high removal efficiency are the criteria for materials to be employed as adsorbents.[39]

In this context, carbon-based aerogels (CAs) are a suitable candidate as an adsorbent for wastewater treatment. The CA is a three-dimensional structure with interconnected graphite sheets and ultralight in weight.[40] CAs possess properties such as large surface area, tunable porosity, high adsorption capacity, rapid adsorption kinetics and reusability.[41–44] CAs were previously used for the removal of pollutant dyes, heavy metal ions, spill of petroleum products and organic solvents from wastewater.[45–48] There are various processes available for the synthesis of CAs. Some are chemical vapour deposition,[49] sol–gel method,[50] biomass pyrolysis,[51] hydrothermal treatment.[49,52] Among them, the biomass pyrolysis method is an appropriate method for the synthesis of highly porous CAs in a single step. Besides this, most of the methods have a complex synthesis process and high cost. The selection of precursor materials for the synthesis of CAs is an essential factor to produce a sustainable and efficient adsorbent. Various precursors used for the synthesis of CAs were reported previously,[53–55] however, these are not environmentally friendly and the cost is also high, so utilization of biomass waste as a precursor material is an appropriate approach to achieve sustainability and cost effectiveness in the synthesis procedures. Additionally, doping of heteroatoms (N, S and P) in CA improves the chemical reactivity of the material.[56]

Herein, an environmentally compatible, cost effective and highly efficient method for the synthesis of a nitrogen-doped carbonaceous aerogel (N-CA) in a simple and single step using waste jaggery as a carbon source is reported. The high active surface area and controlled pore size of the as-synthesized N-CA allow the effective adsorption of pharmaceutical pollutants from wastewater. The removal of ASP and PCM were investigated with the as-synthesized N-CA under various conditions. Further, treated water was explored for the growth of adzuki plants. The sustainable N-CA may also be helpful for several environmental remediation technologies.

2. Experimental section

2.1. Materials

Waste jaggery collected from jaggery mills was utilized as the precursor material. We employed ASP and PCM (target pollutants), hydrochloric acid (HCl) and sodium hydroxide (NaOH) for the pH study and they were purchased from Sigma Aldrich. Ammonium chloride (NH_4Cl) was procured from EMPARTA, India. The adzuki beans utilized in plant growth experiments were purchased from a local market. No additional purification of the drugs and chemicals was required, they were used as received. All the investigations were conducted using distilled water (DI) as the solvent.

2.2. Synthesis of N-CA

The sustainable N-CA was synthesized through a simple process by utilizing waste jaggery as a carbon source.[57,58] Initially, waste jaggery was thoroughly blended with NH_4Cl in a Petri plate. Subsequently, the resulting mixture of waste jaggery and NH_4Cl was placed in a 100 mL silica boat and then put in a hot air oven for heat treatment at 150 °C for a duration of 2 h. After this treatment, a black puffed solid material was produced. Following this, the obtained product was held for 2 h at 700 °C in an argon atmosphere, resulting in the formation of a black, highly porous N-CA. For the reproducibility of the synthesis process, an equal-mass mixture design was followed, wherein 2 grams of waste jaggery were thoroughly mixed with 2 grams of NH_4Cl in a Petri plate. After the completion of the synthesis process, we obtain the final product (N-CA). The standard deviation in mass of N-CA from five batches was found to be ±0.191 gram.

2.3. Instrumentation

In order to gain understanding of the structural and chemical characteristics of the synthesized N-CA, various characterization techniques were employed. Field-emission scanning electron microscopy (FE-SEM) was conducted with a JSM-7500F instrument, operating at 20 kV. For an assessment of the internal morphology and microstructure, transmission electron microscopy (TEM) was performed. Furthermore, a high-resolution transmission electron microscope (HR-TEM) instrument, FEI Tecnai G2 F30 model, operated at 200 kV was utilized to analyse the internal structure of N-CA in detail. The X-ray diffraction (XRD) pattern of N-CA was obtained using a D8-Advance Bruker XRD diffractometer, employing Cu-K_α radiation. X-ray photoelectron spectroscopy

(XPS) was employed to analyse the elements and composition of N-CA using an ESCA$^+$ Omicron Nano Technology instrument from Oxford. The N_2 adsorption isotherm data were noted using an ASiQwin automated gas sorption analyser, Quantachrome Instruments.

2.4. Adsorption experiments

To evaluate the adsorption performance of the synthesized N-CA under natural conditions, ASP and PCM were utilized as model pollutants. So, we first prepared a stock solution of ASP and PCM in DI water, each having a concentration of 1000 mg L^{-1}. The adsorption studies for ASP and PCM were performed using three different parameters, pH value (2 to 12), varying dose (0.25 to 5 mg) and temperature (20 to 60 °C) for the optimization of parameters. Kinetic studies of ASP and PCM adsorption were carried out under optimized conditions, with the concentration of ASP and PCM being 20 mg L^{-1} and 15 mg L^{-1}, respectively. ASP and PCM contaminated samples were stirred with N-CA throughout the adsorption experiment. For the investigation of adsorption isotherms, the contaminated samples of ASP and PCM were prepared having concentrations of 10 to 500 mg L^{-1}. For all the experiments, at regular intervals of 5 minutes, 3 mL of the sample was taken out and a UV-visible spectrophotometer was utilized to measure the absorbance at wavelengths of 298 nm and 244 nm for ASP and PCM, respectively. The removal or adsorption efficiency was evaluated using eqn (1); similarly the ASP and PCM adsorption capacity of N-CA was assessed by using eqn (2).

$$\text{Removal Efficiency}\ (\%) = \frac{C_0 - C_e}{C_0} \times 100 \quad (1)$$

$$\text{Adsorption Capacity}\ \left(\text{mg g}^{-1}\right) = (C_0 - C_e)\,\frac{V}{m} \quad (2)$$

2.5. Spiked water analysis and recycling study

For the real-world applicability and reusability of N-CA, spiked wastewater analysis and recycling study were performed. For this purpose, each targeted pollutant drug was introduced into both tap water and seawater, keeping the conditions consistent with those optimized in DI for ASP and PCM. Following this, a dose of 15 mg of N-CA was supplemented to 10 mL of prepared samples and the previously mentioned procedure was followed (section 2.4). To conduct the recycling study of N-CA, the same adsorption experiments as those for ASP and PCM were performed. However, in the recycling process, the N-CA was collected and subjected to multiple washes with DI water. Afterward, the N-CA was dried at 60 °C and then reused for identical adsorption experiments. Recycling analysis demonstrates the reusability and stability of the adsorbent.

2.6. Ecological assessment of treated water

High quality adzuki beans (*Vigna angularis*) were purchased from the market then thoroughly washed to remove dust and subsequently soaked in five different solutions: DI water, water contaminated with ASP, water contaminated with PCM and treated water after adsorption of ASP and PCM. Afterward, the beans were placed in the same water samples (DI water, ASP-contaminated water, PCM-contaminated water and the treated water) for germination purposes over the course of one day. Then the germinated adzuki beans were allowed to grow in the same Petri plate each containing an equal number of seeds. On the 5th day of the growth period, the growth of adzuki bean plants was observed.

3. Results and discussion

N-CA was synthesized using a waste biomass-based material as shown in Scheme 1.[57,58] This synthesis procedure involves pre-heat treatment followed by post-pyrolysis. In the pre-heat treatment step, a porous aerogel was formed by the process of bubbling. Moreover, during heating NH_4Cl was completely fused with jaggery after undergoing standard cooling procedures and then a solid black product was obtained. Later, the pyrolysis process was conducted for proper carbonization in a split tube furnace and exposed to temperature of up to 700 °C under a regular flow of argon gas (maintaining an inert atmosphere) setting a ramp rate at 5 °C min^{-1}. The pyrolysis process was sustained for 2 h to facilitate complete carbonization after this, allowing for natural cooling. Finally, a highly porous, black N-CA material was obtained and then employed as an adsorbent for ASP and PCM adsorption from wastewater.

3.1. Characterization of the N-doped carbonaceous aerogel

FE-SEM was used to observe the exterior structure of the as-synthesized N-CA. The 3D nano-architecture of the N-CA exhibits an irregular and honeycomb-like highly porous

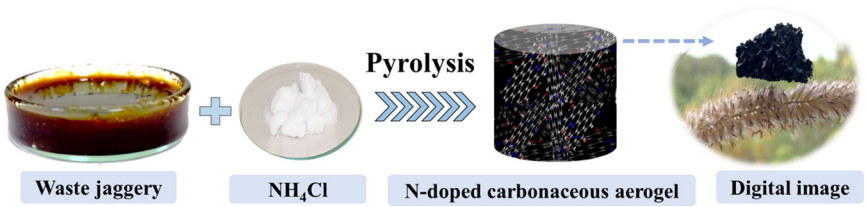

Scheme 1 Schematic of the synthesis of ultralight N-CA using waste jaggery and NH_4Cl as precursors.

structure (Fig. 1a and b).[59] This interconnected hierarchical framework is composed of crumpled disordered carbon nanosheets as depicted in Fig. 1c. The TEM image displayed that N-CA consists of very thin transparent graphitic layers (Fig. 1d).[60] The presence of folds and wrinkles in N-CA shows the 3D flexibility of the disordered carbon (Fig. 1e).[61] The HR-TEM image shows the surface defects in the graphitic structure of N-CA.[59] The interlayer spacing between two disordered graphitic layers was 0.32 nm with respect to the (002) plane shown in Fig. 1f.[62]

In Fig. 2a, the XRD diffraction patterns of the N-CA reveal a prominent broad peak at 25.12°, indicating the presence of disordered graphitic carbon. Another less intense peak was observed at 43.76°, attributed to the graphitic pattern and interlayer formation.[63] The XPS analysis of N-CA revealed the existence of carbon, nitrogen, and oxygen as shown in Fig. 2b. In the deconvoluted C 1s spectrum of N-CA (Fig. 2c), five distinct peaks emerged at binding energies of 284.14, 284.68, 285.43, 286.48 and 289.21 eV. These peaks were attributed to distinct carbon species: C═C sp^2, C–C sp^3, C–O/C═N, C═O/C–N and O═C–O^-. The incorporation of nitrogen into the carbon framework resulted in the presence of C–N bonds. In the O 1s spectrum of N-CA, three distinctive peaks were detected, corresponding to the C═O, C–O and O═C–O^- moieties with a binding energy of 530.72, 532.19 and 533.48 eV, respectively as depicted in Fig. 2d. Furthermore, Fig. 2e presents the high-resolution XPS spectra of N 1s, exhibiting different peaks having a binding energy of 398.20, 400.48 and 401.62 eV ascribed to pyridinic, pyrrolic and graphitic nitrogen present in N-CA, respectively.[57,64] The Brunauer–Emmett–Teller (BET) surface area of N-CA was obtained by using N_2 adsorption and desorption isotherms as shown in Fig. 3a. The specific surface area of N-CA was found to be 1178.18 $m^2\ g^{-1}$ having a pore volume of 1.58 cc g^{-1}.

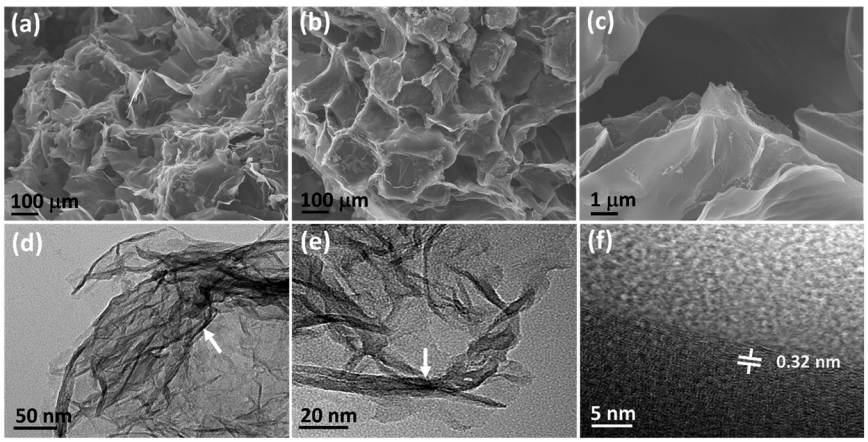

Fig. 1 (a–c) FE-SEM images of N-CA, (d and e) low-magnification TEM images (the white arrow indicates multilayer graphene) and (f) HR-TEM image of N-CA (the white line shows the inter layer distance).

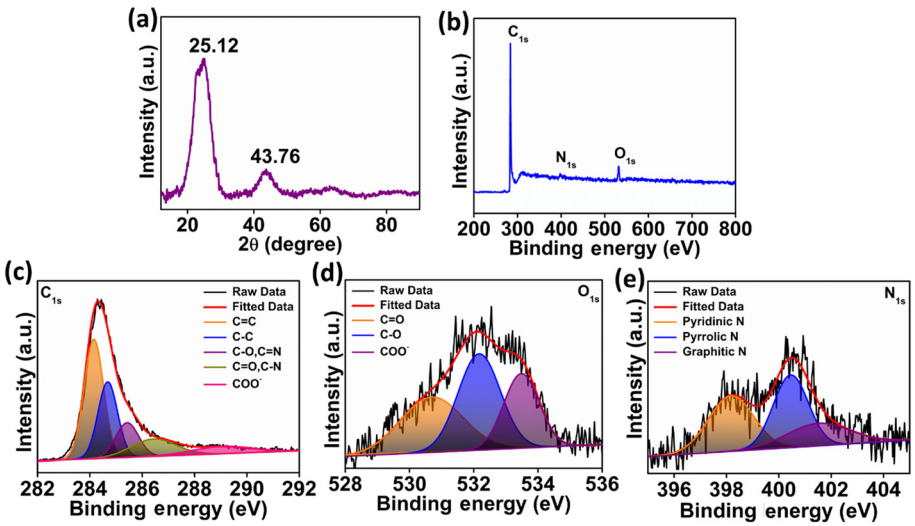

Fig. 2 (a) XRD spectrum of N-CA, (b) XPS survey scan of N-CA, (c) deconvoluted high resolution spectra of C 1s, (d) deconvoluted high resolution spectrum of O 1s and (e) deconvoluted high resolution spectrum of N 1s.

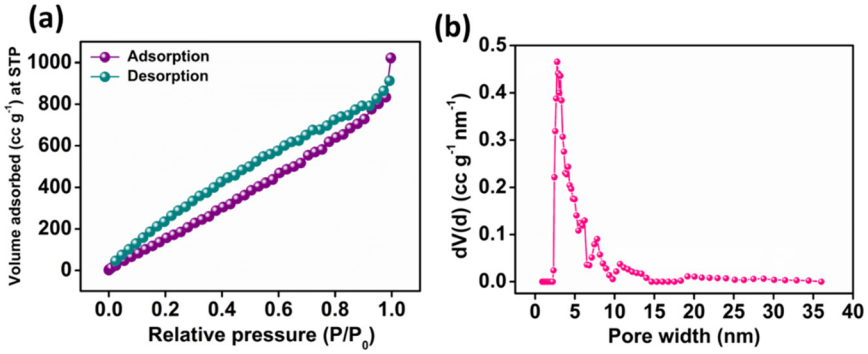

Fig. 3 (a) N_2 adsorption–desorption plot and (b) pore size distribution curve of N-CA.

According to density functional theory (DFT), the pore size distribution in Fig. 3b indicates mesoporous pores (2.76 and 3.16 nm).[65]

3.2. Analysis of the adsorption performance of N-CA

The adsorption of ASP and PCM onto N-CA was analysed under various conditions or parameters. The conditions included variation in pH value, dose, temperature, concentration and retention time.

The impact of the pH value on the adsorption of ASP and PCM is shown in Fig. 4a. First, slowly increasing the pH value brings a slight decline in the adsorption of both ASP and PCM by N-CA within the pH of 2 to 4. Afterward, as the pH gradually increased from 4 to 12, there was a consistent reduction in the adsorption of ASP and PCM.[66] This decrease can be due to the diminishing π–π bonding between the drug and the N-CA (as an adsorbent). The influence of N-CA doses on the adsorption of ASP having a concentration of 20 mg L^{-1} and PCM with a 15 mg L^{-1} concentration was investigated. A dose of N-CA starting from 2.5 to 50 mg was added to 10 mL of sample. At first, as the N-CA dose was increased from 0.25 to 1.5 mg mL^{-1} there was a clear enhancement in the removal efficiency as shown in Fig. 4b. The enhancement can be accredited to the larger surface area and a high number of active sites are available for adsorption on the N-CA.[67] Finally, the observations showed that the optimum N-CA dose for ASP and PCM adsorption was 1.5 mg mL^{-1}. After a 1.5 mg mL^{-1} dose, the removal efficiency remains constant, which indicates that there is no rise in the removal of ASP and PCM. The effect of temperature on the adsorption of ASP and PCM was studied. Temperature is an essential factor in affecting the adsorption capacity of N-CA for pharmaceutical substances.[66] The temperature-dependent removal efficiency is presented in Fig. 4c. As the temperature of the solution gradually increased from 20 to 60 °C, there was a minor reduction in the removal efficiency of both ASP and PCM. These temperature-dependent outcomes are used to calculate the thermodynamic parameters and isotherms of the adsorption process. A retention time investigation was conducted to analyse the adsorption of ASP and PCM on N-CA over time. It was observed that in the initial stage, there was a quick rise in the removal efficiency by N-CA, then reached a plateau after ~40 min.[68] This rapid adsorption at the initial stage can be because of the complete availability of the number of active sites on N-CA for the adsorption of ASP and PCM. However, after some time the number of available active sites on N-CA became gradually filled with ASP and PCM. Fig. 4d depicts the removal efficiency of N-CA over time for ASP and PCM.

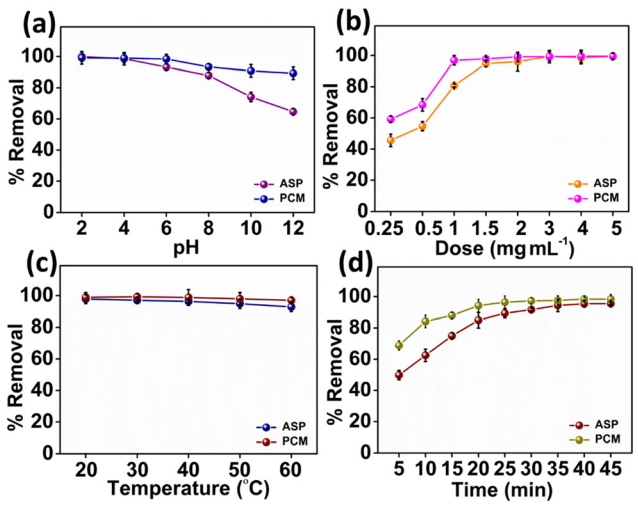

Fig. 4 Plot of the percentage removal/adsorption of ASP and PCM with parameters: (a) pH, (b) dose, (c) temperature and (d) time.

3.3. Kinetic studies

A comprehensive kinetic study was conducted to analyse the adsorption behaviour of ASP and PCM on the N-CA. The absorbance spectra (ASP and PCM) for the control and after 40 minutes of adsorption under optimized conditions are depicted in Fig. S1.† For the adsorption kinetics, two models were utilized, first is the pseudo-first-order (PFO) kinetics mathematically represented by eqn (3) and the other is the pseudo-second-order (PSO) kinetics expressed in eqn (4), respectively.[69]

$$\ln(q_e - q_t) = \ln q_e - k_1 t \quad (3)$$

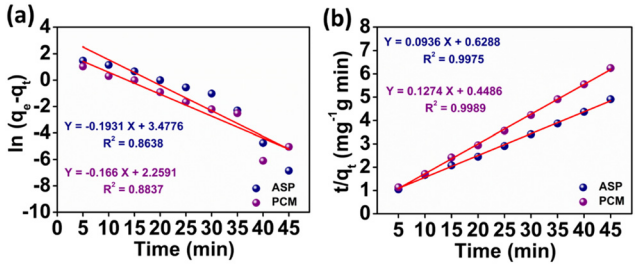

Fig. 5 Plot of the adsorption kinetics of ASP and PCM: (a) pseudo first order and (b) pseudo second order.

$$\frac{t}{q_t} = \frac{1}{k_2 q_e^{\,2}} + \frac{t}{q_e} \tag{4}$$

where k_1 signifies the PFO rate constant, while k_2 denotes the PSO rate constant. The determination of k_1 and k_2 was performed by plotting $\ln(q_e - q_t)$ against retention time, t and t/q_t against t, respectively. The kinetic parameters (k_1 and k_2 values) obtained from the aforementioned kinetic models (eqn (3) and (4)) provide the insight of adsorption. The kinetic plots for ASP and PCM reveal R^2 values of 0.8638 and 0.8837, respectively, for the PFO model (Fig. 5a). R^2 values indicate that the experimental data do not fit into the PFO model. On the other hand, in Fig. 5b, the R^2 values for the PSO kinetic model were calculated as 0.9975 for ASP and 0.9989 for PCM. This signifies the best linear fitting between the experimental results and the PSO model. Moreover, the calculated adsorption capacity ($q_{e,cal}$) obtained from the PSO kinetic model closely matched with the experimental values ($q_{e,exp}$), demonstrating the excellent fitting of this model to the experimental data. The kinetic parameters along with their respective R^2 values are presented in Table S1.†

3.4. Adsorption isotherms

With the help of adsorption isotherms, we can express in which way an adsorbate is distributed between a solid surface and a liquid phase. The Langmuir isotherm suggests that the monolayer adsorption occurs on the uniform surface of the adsorbent, where a constant number of adsorption sites exist on the outer surface of any adsorbent material. The Langmuir equation,[70] denoted in its linear form as eqn (5), can be expressed as follows:

$$\frac{C_e}{q_e} = \frac{C_e}{q_m} + \frac{1}{q_m K_L} \tag{5}$$

where C_e (mg L^{-1}) is the concentration of ASP and PCM at equilibrium, q_m (mg g^{-1}) indicates the maximum adsorption capacity for monolayer formation and K_L (mg g^{-1}) stands for the Langmuir constant.

Another isotherm model, the Freundlich isotherm model, was employed to define the adsorption phenomenon, which involves multilayer adsorption on the heterogeneous active sites of N-CA. The Freundlich model can be expressed in the following eqn (6).[71]

$$\ln q_e = \ln K_F + \frac{1}{n} \ln C_e \tag{6}$$

where q_e (mg g^{-1}) is the amount of adsorbed ASP and PCM at equilibrium, K_F (mg g^{-1}) is the Freundlich constant, n is the Freundlich exponent and C_e (mg L^{-1}) is the equilibrium concentration of ASP and PCM.

The observed adsorption isotherm results for ASP and PCM were subjected to fitting with both Langmuir and Freundlich isotherm models. In Fig. 6a, the adsorption of ASP and PCM onto N-CA closely fitted to the Langmuir model as indicated by R^2 values of 0.9842 for ASP and 0.9973 for PCM. However, when the experimental data subjected to fit into the Freundlich model, the obtained R^2 values for ASP and PCM were 0.8305 and 0.9133, respectively (Fig. 6b). According to the observations, it is found that as the equilibrium concentration (C_e) increases, the equilibrium adsorption capacity (q_e) increased as depicted in Fig. 7a. All parameters obtained from the Langmuir and Freundlich isotherms are mentioned in Table S2.† The maximum adsorption capacity (q_m) of N-CA was determined as 138.6963 ± 7.8687 mg g^{-1} for ASP and 117.7856 ± 2.7219 mg g^{-1} for PCM. For the comparative study, another experiment was performed for the adsorption of ASP and PCM using commercially available graphene oxide (GO) under the same experimental conditions. The adsorption efficiencies of GO toward ASP and PCM were ~71% and ~74%, respectively, as shown in Fig. S2.† A comparison of the maximum adsorption capacity of N-CA with carbon-based and other adsorbents for ASP and PCM is given in Table 1.

The adsorption of ASP and PCM on N-CA follows the Langmuir adsorption isotherm. Further, the Langmuir separation factor (R_L) is calculated using eqn (7),[83] and can be expressed as follows:

$$R_L = \frac{1}{1 + K_L C_0} \tag{7}$$

where K_L represents the Langmuir constant and C_0 denotes the initial concentrations of ASP and PCM. When the R_L values range from 0 to 1, it signifies a favourable adsorption process.[84] From eqn (7), the calculated R_L values for ASP and PCM were 0.57 and 0.21, respectively. These outcomes indicate that the adsorption of ASP and PCM by N-CA was favourable.

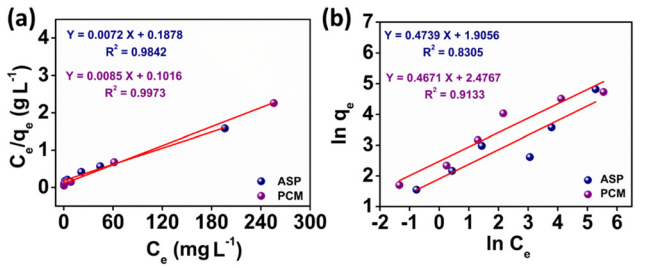

Fig. 6 Plot of the adsorption isotherms of ASP and PCM: (a) Langmuir and (b) Freundlich.

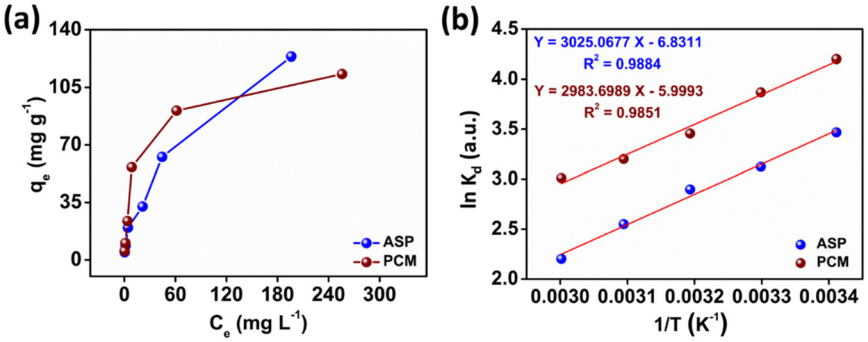

Fig. 7 The relationship between (a) q_e *vs.* C_e and (b) ln K_d *vs.* 1/T.

Table 1 Adsorption of ASP and PCM with the as-synthesized N-CA compared with various adsorbents

Adsorbent	Adsorbate	q_m (mg g^{-1})	Ref.
Reduced GO	ASP	21.41	72
Graphitic-C_3N_4	ASP	21.27	73
Graphene nanoplates	ASP	12.98	74
Pristine multiwall CNTs (PMCNT)	ASP	41.00	75
Functionalized CNTs (FMCNT)	ASP	58.00	75
AC from babassu coconut mesocarp	ASP	89.87	76
Tannin and kraft black liquor (RFA)	ASP	50.17	77
Tannin and kraft black liquor (RFC)	ASP	91.66	77
N-CA	ASP	138.69	This work
Orange rind derived GO	PCM	0.542	78
Palm kernel shell derived GO	PCM	0.584	78
Graphene nanoplates	PCM	18.07	74
AC from *Butia capitata* (high temp)	PCM	98.19	79
AC from *Butia capitata* (low temp)	PCM	73.00	79
AC from *Cannabis sativa*	PCM	16.18	80
N-CNT-β-CD	PCM	41.00	81
Fe/N-CNT-β-CD	PCM	75.2	81
Tannin and kraft black liquor (RFA)	PCM	49.95	77
Tannin and kraft black liquor (RFC)	PCM	73.58	77
Spent tea leaves (STL-ACH)	PCM	59.2	82
N-CA	PCM	117.78	This work

3.5. Thermodynamic isotherms

The parameters of thermodynamics involved in adsorption of ASP and PCM onto N-CA were calculated using eqn (8)–(10).[85–87]

$$K_d = \frac{q_e}{C_e} \quad (8)$$

$$\ln K_d = \frac{\Delta S^\circ}{R} - \frac{\Delta H^\circ}{RT} \quad (9)$$

$$\Delta G^\circ = \Delta H^\circ - T\Delta S^\circ \quad (10)$$

where K_d represents the distribution coefficient, ΔS° denotes the entropy change (J mol^{-1} K^{-1}), R signifies the universal gas constant (8.314 J mol^{-1} K^{-1}), ΔH° stands for the enthalpy change (kJ mol^{-1}), T corresponds to the temperature (Kelvin) and ΔG° represents the free energy change (kJ mol^{-1}). Fig. 7b depicts a linear correlation between ln K_d and 1/T and the ΔH° value was obtained from the slope and ΔS° was obtained from the intercept of the linearly fitted plot. The values of the thermodynamic parameters, ΔS°, ΔH° and ΔG°, are mentioned in Table 2. The positive values of ΔH° and ΔS° indicate the endothermic nature of ASP and PCM adsorption and increase in randomness throughout the adsorption. According to the obtained calculations of ΔH° and ΔS°, we found negative ΔG° values which signify the spontaneous adsorption of ASP and PCM on N-CA.

4. Spiked sample analysis and recycle study

To evaluate the adsorption of ASP and PCM from the spiked water sample, we introduced ASP and PCM into tap water and seawater. The experiment was performed under previously mentioned optimized conditions. Herein, the N-CA demonstrated nearly identical removal efficiencies to DI water for ASP and PCM in both tap and seawater spiked samples as shown in Fig. 8a. The performance of N-CA in adsorption across different types of water highlights its promising practical applicability. Moreover, the reusability of N-CA for removal of ASP and PCM from wastewater was maintained up to ~79% and

Table 2 Thermodynamic parameters for the adsorption of ASP and PCM with N-CA

	ΔS° (J mol^{-1} K^{-1})	ΔH° (kJ mol^{-1})	ΔG° (kJ mol^{-1})				
			293.15 K	303.15 K	313.15 K	323.15 K	333.15 K
ASP	56.79	25.15	−16.62	−17.19	−17.75	−18.32	−18.89
PCM	49.87	24.80	−14.60	−15.10	−15.59	−16.09	−16.59

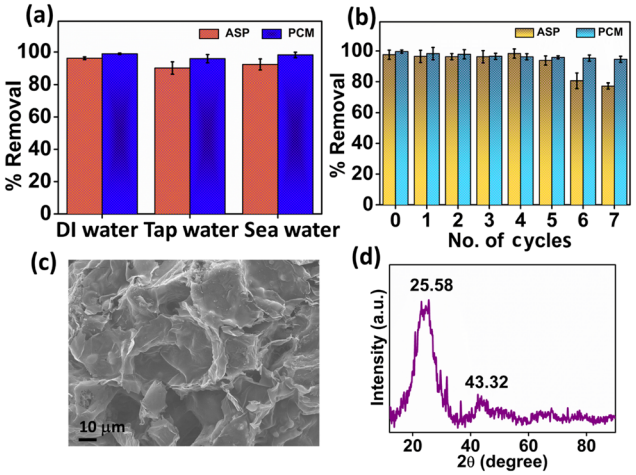

Fig. 8 (a) Percentage removal efficiency of ASP and PCM in spiked water and (b) recycling study of N-CA. Characterization of N-CA after adsorption studies. (c) FE-SEM image of N-CA and (d) XRD spectrum of N-CA after adsorption.

~95% respectively until seven cycles as shown in Fig. 8b. After each adsorption cycle, the N-CA was collected, washed with DI water and later dried in an oven.

After adsorption studies, washing and drying were performed and then post-characterization (FE-SEM and XRD) was conducted to inspect the chemical and structural stability of the adsorbent material. The FE-SEM image (Fig. 8c) after adsorption of ASP shows that there are no changes in the morphology of N-CA and the pore structure is similar to that of the as-synthesized material. The XRD diffraction pattern of N-CA in Fig. 8d after the adsorption of ASP displays two peaks, which are the same as the synthesized material. This indicates that there is no change in the phase even after adsorption. These post-characterization findings clearly showed that the structural and chemical properties of N-CA (as an adsorbent) remain unchanged even after adsorption.

5. Assessment of the effect of treated water on adzuki bean growth

For the evaluation of the germination rate, adzuki beans were immersed in different water samples: DI water (used as a control), water contaminated with ASP and PCM solutions and ASP and PCM water treated with N-CA.[88] In the case of the ASP contaminated water, the germination rate was ~64%, while for the PCM contaminated water it was 0%, as depicted in Fig. 9a. There was a slight increase in the germination rate when treated water (after ASP adsorption with N-CA) reached ~92% as compared to DI water (77%). After adsorption of PCM by N-CA, the treated water has a germination rate of ~86%. For the growth profile analysis,[89] germinated adzuki beans were cultivated in DI water, water contaminated with ASP and PCM and treated water after the adsorption of ASP and PCM with N-CA over the intervals of 5 days. The shoot and root length of the adzuki plant was obserbed to show a trend similar to the germination rate after 5 days of germination. In ASP and PCM contaminated water significantly shorter shoot and root lengths were observed as depicted in Fig. 9b. Both the shoot and root lengths were found to be shorter in the control as compared to treated water after the adsorption of ASP and PCM with

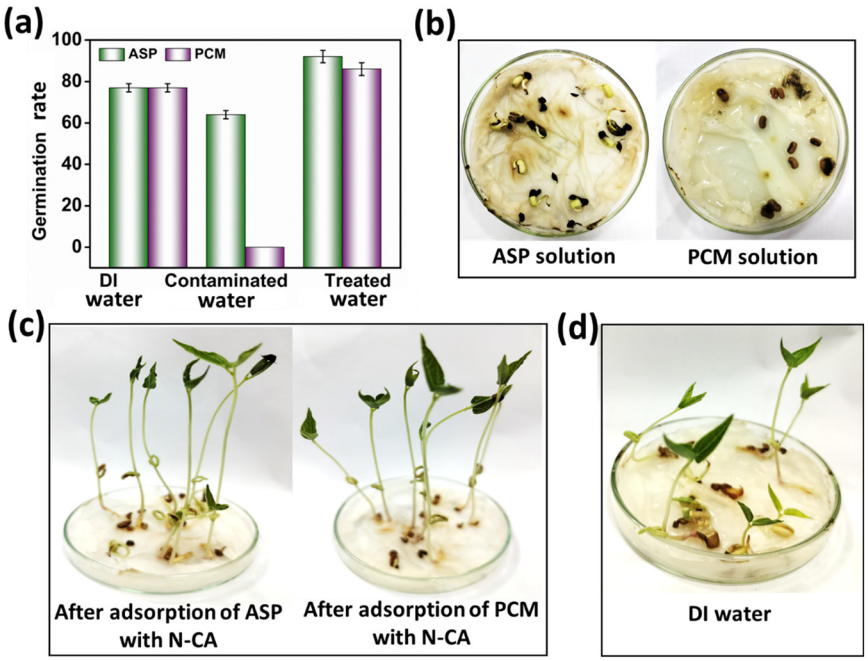

Fig. 9 The growth of adzuki plants after 5 days under different conditions: (a) germination rate, (b) ASP and PCM solutions, (c) after adsorption of ASP and PCM with N-CA and (d) DI water (control).

N-CA. Observations revealed that ASP and PCM containing germinated seeds suppressed the growth of adzuki plants. In contrast, adzuki bean plants grown after the adsorption of ASP and PCM with N-CA exhibited improved growth compared to the DI water grown plants (Fig. 9c). The growth pattern of adzuki bean plants in DI water (control) is shown in Fig. 9d. The substantial growth enhancement in water treated with N-CA strongly supports its non-toxic impact on plant development. Furthermore, this approach holds promise for the reuse of treated wastewater.

Conclusion

N-CA was successfully synthesized by using waste jaggery through a straightforward, one-step and facile pyrolysis process. The as-synthesized N-CA possesses a three-dimensional nanostructured arrangement with large surface area and high porosity, which is essential for any adsorbent. Herein, N-CA serves as an effective adsorbent for the removal of ASP and PCM drugs under natural environmental conditions. Within 40 minutes, the N-CA achieved an impressive adsorption rate of ~96% of ASP and ~99% of PCM. The adsorption kinetics of ASP and PCM follows the PSO kinetics model. In adsorption isotherm investigations, the obtained experimental data were more accurately fitted into the Langmuir isotherm adsorption model. The practical applicability of the N-CA was evaluated in tap water and seawater, revealing no significant change in the adsorption of ASP and PCM as compared to DI water. Furthermore, the N-CA revealed excellent reusability up to seven cycles and recovery of the adsorbent is easy without using the filtration process. The characterization of N-CA after the adsorption of ASP showed the excellent stability of the material after the seventh cycle. Later, the treated water was utilized for the germination of adzuki beans and growth of plants; the outcomes showed ~92% germination rate for both ASP and PCM. These findings suggest that the treated water possesses significant potential for fulfilling water needs in construction sites, road side plantations and agricultural fields.

Conflicts of interest

There are no conflicts to declare.

Acknowledgements

H. A. is grateful to IIPE Visakhapatnam for the doctoral fellowship. R. M. thanks IIPE for funding (IIPE/DORD/IRG/10). K. M. T. concedes financial assistance from the Department of Biotechnology (DBT), India, through the RamalingaswamiFaculty Award (BT/RLF/Re-entry/45/2018). Authors acknowledge SBIF XRD analytical laboratory, IIPE for HR-XRD facility.

References

1 C. Luo, M. Feng, V. K. Sharma and C.-H. Huang, *Environ. Sci. Technol.*, 2019, **53**, 5272–5281.
2 P. Regkouzas and E. Diamadopoulos, *Chemosphere*, 2019, **224**, 840–851.
3 E. Nyankson, J. K. Efavi, B. Agyei-Tuffour and G. Manu, *RSC Adv.*, 2021, **11**, 17032–17045.
4 S. K. Fanourakis, J. Peña-Bahamonde, P. C. Bandara and D. F. Rodrigues, *npj Clean Water*, 2020, **3**, 1.
5 J. Sun, C. Jiang, Z. Wu, Y. Liu and S. Sun, *Chemosphere*, 2022, **308**, 136107.
6 M. Patel, R. Kumar, K. Kishor, T. Mlsna, C. U. Pittman, Jr. and D. Mohan, *Chem. Rev.*, 2019, **119**, 3510–3673.
7 J. N'Diaye, S. Poorahong, O. Hmam, G. C. Jiménez, R. Izquierdo and M. Siaj, *Membranes*, 2020, **10**, 340.
8 L. Bírošová, K. Lépesová, R. Grabic and T. Mackuľak, *Environ. Sci. Pollut. Res.*, 2020, **27**, 13501–13511.
9 M. F. Meyer, S. M. Powers and S. E. Hampton, *Environ. Sci. Technol.*, 2019, **53**, 12961–12973.
10 L. D. Freitas and G. Radis-Baptista, *J. Xenobiot.*, 2021, **11**, 61–76.
11 L. F. Angeles, R. A. Mullen, I. J. Huang, C. Wilson, W. Khunjar, H. I. Sirotkin, A. E. McElroy and D. S. Aga, *Environ. Sci.: Water Res. Technol.*, 2020, **6**, 62–77.
12 J. Mei, C. Wang, L. Kong, P. Sun, Q. Hu, H. Zhao, Y. Guo and S. Yang, *J. Hazard. Mater.*, 2020, **381**, 120967.
13 K. M. Lee, C. W. Lai, K. S. Ngai and J. C. Juan, *Water Res.*, 2016, **88**, 428–448.
14 X. Li, Z. Kuang, J. Zhang, X. Liu, J. Hu, Q. Xu, D. Wang, Y. Liu, Q. Wang, Q. Yang and H. Li, *ACS Sustainable Chem. Eng.*, 2020, **8**, 8681–8691.
15 N. Suzuki, A. Okazaki, H. Kuriyama, I. Serizawa, Y. Hirami, A. Hara, Y. Hirano, Y. Nakabayashi, N. Roy, C. Terashima, K. Nakata, K.-i. Katsumata, T. Kondo, M. Yuasa and A. Fujishima, *RSC Adv.*, 2020, **10**, 1793–1798.
16 H. Cui, X. Huang, Z. Yu, P. Chen and X. Cao, *RSC Adv.*, 2020, **10**, 20231–20244.
17 H. T. Van, V. H. Hoang, T. C. Luu, T. L. Vi, L. T. Q. Nga, G. S. I. J. Marcaida and T.-T. Pham, *RSC Adv.*, 2023, **13**, 28753–28766.
18 F. Dolatkhah, T. Mohammadi and M. A. Tofighy, *J. Water Process Eng.*, 2022, **50**, 103222.
19 K. Govindan, A. Angelin, M. Kalpana, M. Rangarajan, P. Shankar and A. Jang, *ACS Appl. Mater. Interfaces*, 2020, **12**, 1775–1788.
20 B. Lee, Y. Baek, M. Lee, D. H. Jeong, H. H. Lee, J. Yoon and Y. H. Kim, *Nat. Commun.*, 2015, **6**, 7109.
21 J. K. H. Wong, H. K. Tan, S. Y. Lau, P.-S. Yap and M. K. Danquah, *J. Environ. Chem. Eng.*, 2019, **7**, 103261.
22 Y. Zeng, X. Zhan, B. Hong, Y. Xia, Y. Ding, T. Cai, K. Yin, X. Wang, L. Yang and S. Luo, *Chem. Eng. J.*, 2023, **452**, 139434.
23 R. Rashid, I. Shafiq, P. Akhter, M. J. Iqbal and M. Hussain, *Environ. Sci. Pollut. Res.*, 2021, **28**, 9050–9066.
24 A. E. Burakov, E. V. Galunin, I. V. Burakova, A. E. Kucherova, S. Agarwal, A. G. Tkachev and V. K. Gupta, *Ecotoxicol. Environ. Saf.*, 2018, **148**, 702–712.
25 J. R. de Andrade, M. F. Oliveira, M. G. C. da Silva and M. G. A. Vieira, *Ind. Eng. Chem. Res.*, 2018, **57**, 3103–3127.

26 Momina and K. Ahmad, *J. Cleaner Prod.*, 2023, **388**, 136014.
27 A. K. Badawi, M. Abd Elkodous and G. A. M. Ali, *RSC Adv.*, 2021, **11**, 36528–36553.
28 A. Srivastava, B. Gupta, A. Majumder, A. K. Gupta and S. K. Nimbhorkar, *J. Environ. Chem. Eng.*, 2021, **9**, 106177.
29 R. M. C. Viegas, A. S. Mestre, E. Mesquita, M. Campinas, M. A. Andrade, A. P. Carvalho and M. J. Rosa, *Sci. Total Environ.*, 2020, **743**, 140791.
30 P. Arabkhani, H. Javadian, A. Asfaram and M. Ateia, *Chemosphere*, 2021, **271**, 129610.
31 T. De Oliveira, E. Fernandez, L. Fougère, E. Destandau, M. Boussafir, M. Sohmiya, Y. Sugahara and R. Guégan, *ACS Omega*, 2018, **3**, 15332–15342.
32 M. Alnajjar, A. Hethnawi, G. Nafie, A. Hassan, G. Vitale and N. N. Nassar, *J. Environ. Chem. Eng.*, 2019, **7**, 102994.
33 A. Jahanban-Esfahlan, R. Jahanban-Esfahlan, M. Tabibiazar, L. Roufegarinejad and R. Amarowicz, *RSC Adv.*, 2020, **10**, 7026–7047.
34 Y. Wang, X. Wei, R. Zhang, Y. Wu, M. U. Farid and H. Huang, *RSC Adv.*, 2017, **7**, 52719–52728.
35 J. Li, L. Wang, Y. Liu, P. Zeng, Y. Wang and Y. Zhang, *ACS Omega*, 2020, **5**, 27962–27971.
36 Y. Chen, J. Shi, Q. Du, H. Zhang and Y. Cui, *RSC Adv.*, 2019, **9**, 14143–14153.
37 F. Hokmabadi, R. Zadmard, M. R. Jalali and M. S. Abaee, *RSC Adv.*, 2022, **12**, 25123–25132.
38 P. Kumari, K. M. Tripathi, K. Awasthi and R. Gupta, *Environ. Sci. Pollut. Res.*, 2023, **30**, 15480–15489.
39 M. J. Uddin and Y.-K. Jeong, *Environ. Sci. Pollut. Res.*, 2020, **27**, 39888–39912.
40 Y. Chen, L. Yang, S. Xu, S. Han, S. Chu, Z. Wang and C. Jiang, *RSC Adv.*, 2019, **9**, 22950–22956.
41 K. Li, M. Zhou, L. Liang, L. Jiang and W. Wang, *J. Colloid Interface Sci.*, 2019, **546**, 333–343.
42 Y. Lv, Z. Liang, Y. Li, Y. Chen, K. Liu, G. Yang, Y. Liu, C. Lin, X. Ye, Y. Shi and M. Liu, *Environ. Res.*, 2021, **194**, 110652.
43 X. Liu, K. Pang, H. Yang and X. Guo, *Carbon*, 2020, **161**, 146–152.
44 D. Zhao, Y. Wang, S. Zhao, M. Wakeel, Z. Wang, R. S. Shaikh, T. Hayat and C. Chen, *Environ. Pollut.*, 2019, **251**, 547–554.
45 T. H. Tu, P. T. N. Cam, L. V. T. Huy, M. T. Phong, H. M. Nam and N. H. Hieu, *Mater. Lett.*, 2019, **238**, 134–137.
46 Y. Zhang, L. Wu, H. Deng, N. Qiao, D. Zhang, H. Lin and Y. Chen, *J. Environ. Chem. Eng.*, 2021, **9**, 106008.
47 Y. Zhuang, S. Tang, W. Shen, F. Yang and H. K. Lee, *TrAC, Trends Anal. Chem.*, 2023, **168**, 117352.
48 M. Pan, C. Shan, X. Zhang, Y. Zhang, C. Zhu, G. Gao and B. Pan, *Environ. Sci. Technol.*, 2018, **52**, 739–746.
49 S. Long, H. Wang, K. He, C. Zhou, G. Zeng, Y. Lu, M. Cheng, B. Song, Y. Yang, Z. Wang, X. Luo and Q. Xie, *Colloids Surf., A*, 2020, **594**, 124666.
50 H. Yang, Z. Li, B. Lu, J. Gao, X. Jin, G. Sun, G. Zhang, P. Zhang and L. Qu, *ACS Nano*, 2018, **12**, 11407–11416.
51 X. Kong, Y. Zhu, H. Lei, C. Wang, Y. Zhao, E. Huo, X. Lin, Q. Zhang, M. Qian, W. Mateo, R. Zou, Z. Fang and R. Ruan, *J. Chem. Eng.*, 2020, **399**, 125808.
52 K. Hu, T. Szkopek and M. Cerruti, *J. Mater. Chem. A*, 2017, **5**, 23123–23130.
53 S. Ye, Y. Liu and J. Feng, *ACS Appl. Mater. Interfaces*, 2017, **9**, 22456–22464.
54 C. Chen, X. Zhu and B. Chen, *Chem. Eng. J.*, 2018, **354**, 896–904.
55 S. Yang, L. Zhang, Q. Yang, Z. Zhang, B. Chen, P. Lv, W. Zhu and G. Wang, *J. Mater. Chem. A*, 2015, **3**, 7950–7958.
56 Z. Li, J. Lin, B. Li, C. Yu, H. Wang and Q. Li, *J. Energy Storage*, 2021, **44**, 103437.
57 V. K. Bajpai, S. Shukla, I. Khan, S.-M. Kang, Y. Haldorai, K. M. Tripathi, S. Jung, L. Chen, T. Kim, Y. S. Huh and Y.-K. Han, *ACS Appl. Mater. Interfaces*, 2019, **11**, 43949–43963.
58 H. Asati, R. Mondal and K. M. Tripathi, *Environ. Sci.: Nano*, 2024, DOI: **10.1039/D3EN00752A**.
59 S. Shukla, I. Khan, V. K. Bajpai, H. Lee, T. Kim, A. Upadhyay, Y. S. Huh, Y.-K. Han and K. M. Tripathi, *ACS Appl. Mater. Interfaces*, 2019, **11**, 18165–18177.
60 C. Maouche, Y. Zhou, J. Peng, S. Wang, X. Sun, N. Rahman, P. Yongphet, Q. Liu and J. Yang, *RSC Adv.*, 2020, **10**, 12423–12431.
61 X. Shi, J. Zhu, Y. Zhang, S. He, Y. Bi and L. Zhang, *RSC Adv.*, 2015, **5**, 77130–77137.
62 J. Kaushik, V. Kumar, A. K. Garg, P. Dubey, K. M. Tripathi and S. K. Sonkar, *New J. Chem.*, 2021, **45**, 9073–9083.
63 T. Imboon, J. Khumphon, K. Yotkuna, I. M. Tang and S. Thongmee, *SN Appl. Sci.*, 2021, **3**, 653.
64 M. Park, A. Sharma, C. Kang, J. Han, K. M. Tripathi and H.-J. Lee, *ACS Biomater. Sci. Eng.*, 2022, **8**, 2131–2141.
65 Y. Myung, S. Jung, T. T. Tung, K. M. Tripathi and T. Kim, *ACS Sustainable Chem. Eng.*, 2019, **7**, 3772–3782.
66 T. Qiu, J.-G. Yang, X.-J. Bai and Y.-L. Wang, *RSC Adv.*, 2019, **9**, 12737–12746.
67 H. Zhu, T. Chen, J. Liu and D. Li, *RSC Adv.*, 2018, **8**, 2616–2621.
68 P. Kumari, K. M. Tripathi, K. Awasthi and R. Gupta, *Ind. Eng. Chem. Res.*, 2023, **62**, 13837–13847.
69 J. Zhao, L. Yu, F. Zhou, H. Ma, K. Yang and G. Wu, *RSC Adv.*, 2021, **11**, 8025–8032.
70 W. Sun, W. Zhang, H. Li, Q. Su, P. Zhang and L. Chen, *RSC Adv.*, 2020, **10**, 8790–8799.
71 T. L. Tan, P. A. P. Krusnamurthy, H. Nakajima and S. A. Rashid, *RSC Adv.*, 2020, **10**, 18740–18752.
72 A. Zaka, T. Ibrahim and M. Khamis, *Desalin. Water Treat.*, 2021, **212**, 401–414.
73 M. Chegeni, Z. Mousavi, M. Soleymani and S. Dehdashtian, *Diamond Relat. Mater.*, 2020, **101**, 107621.
74 L. A. Al-Khateeb, S. Almotiry and M. A. Salam, *J. Chem. Eng.*, 2014, **248**, 191–199.
75 M. R. Elamin, B. Y. Abdulkhair and A. O. Elzupir, *Sci. Rep.*, 2019, **9**, 12795.

76 M. I. Hoppen, K. Q. Carvalho, R. C. Ferreira, F. H. Passig, I. C. Pereira, R. C. P. Rizzo-Domingues, M. K. Lenzi and R. C. R. Bottini, *J. Environ. Chem. Eng.*, 2019, **7**, 102862.
77 W. Martins Moreira, P. V. Viotti, M. G. A. Vieira, C. M. dos Santos Gaudêncio Baptista, M. H. Neves Olsen Scaliante and M. L. Gimenes, *Colloids Surf., A*, 2021, **608**, 125597.
78 T. M. Osobamiro and A. Oladipo, *Annals of Science and Technology*, 2022, **7**, 69–75.
79 C. Yanan, Z. Srour, J. Ali, S. Guo, S. Taamalli, V. Fèvre-Nollet, K. da Boit Martinello, J. Georgin, D. S. P. Franco, L. F. O. Silva, G. L. Dotto, A. Erto, F. Louis, A. E. Bakali and L. Sellaoui, *J. Chem. Eng.*, 2023, **454**, 139943.
80 M. Sajid, S. Bari, M. Saif Ur Rehman, M. Ashfaq, Y. Guoliang and G. Mustafa, *Alexandria Eng. J.*, 2022, **61**, 7203–7212.
81 K. Mphahlele, M. S. Onyango and S. D. Mhlanga, *J. Environ. Chem. Eng.*, 2015, **3**, 2619–2630.
82 S. Wong, Y. Lim, N. Ngadi, R. Mat, O. Hassan, I. M. Inuwa, N. B. Mohamed and J. H. Low, *Powder Technol.*, 2018, **338**, 878–886.
83 R. Singh and R. Bhateria, *ACS Omega*, 2020, **5**, 10826–10837.
84 Saruchi, M. Sharma, M. R. Hatshan, V. Kumar and A. Rana, *J. Chem. Eng. Data*, 2021, **66**, 646–657.
85 S. A. Khan, M. F. Siddiqui and T. A. Khan, *ACS Omega*, 2020, **5**, 2843–2855.
86 N. Mojoudi, N. Mirghaffari, M. Soleimani, H. Shariatmadari, C. Belver and J. Bedia, *Sci. Rep.*, 2019, **9**, 19352.
87 G. Özsin, M. Kılıç, E. Apaydın-Varol and A. E. Pütün, *Appl. Water Sci.*, 2019, **9**, 56.
88 S. J. Park, G. S. Das, F. Schütt, R. Adelung, Y. K. Mishra, K. M. Tripathi and T. Kim, *NPG Asia Mater.*, 2019, **11**, 8.
89 Gunture, A. Singh, A. Bhati, P. Khare, K. M. Tripathi and S. K. Sonkar, *Sci. Rep.*, 2019, **9**, 2522.